International Journal of Environmental Sciences & Natural Resources
ISSN: 2572-1119

Juniper Publishers
key to the Researchers

Research Article
Volume 22 Issue 5 - December 2019
DOI: 10.19080/IJESNR.2019.22.556098

Int J Environ Sci Nat Res

Coastal Land Dynamics and Vulnerability Analyses based on the Brightness-Greenness-Wetness Model

Xuelian Meng[1,2]* and Haitian Zhu[1,3]

[1]*Department of Geography and Anthropology, Louisiana State University, USA*

[2]*Coastal Studies Institute, Louisiana State University, USA*

[3]*National Satellite Ocean Application Service (NSOAS), State Oceanic Administration, China*

Submission: November 25, 2019; **Published:** December 04, 2019

***Corresponding author:** Xuelian Meng, Department of Geography and Anthropology, Louisiana State University, Baton Rouge, LA 70803 & Coastal Studies Institute, Louisiana State University, Baton Rouge, LA 70803, USA

Abstract

This paper introduces the simplified brightness-greenness-wetness (B-G-W) model for multi-temporal land dynamics and vulnerability analyses in coastal environments and searches for an optimal mapping solution based on Landsat images to support its applications. A comparative study using the machine-learning algorithm of Support Vector Machine (SVM) first evaluated different sets of input bands (DN, KTC transformation, and different indices) and compared pixel- vs. object-based approaches to select an accurate and robust classification approach. The adoption of a recently developed multi-scale analysis method helped to quantify and identify the optimal segmentation scale for object-based classification. The results indicated that pixel-based SVM classification based on KTC transformation produced the most reliable performance with an overall accuracy of 95.85% and a kappa value of 0.9333. In addition, object-based approach demonstrated no advantage in mapping fragmented landscapes with the B-G-W model. This research then applied the method to decadal land dynamics analysis in the Mississippi River bird's-foot delta based on January images in 1973, 1983, 1994, 2003, and 2014. The vulnerability analysis through land-change frequency mapping indicates stable lands, most vulnerable areas, and vulnerable areas with potential for wetland conservation..

Keywords: Decadal land dynamics; SVM; Pixel- and object-based classification; Multi-scale segmentation; B-G-W model

Introduction

Coastal wetlands are among the highest productive ecosystems, supporting rich habitats for human settlements, plants, fish, shellfish, plankton, and other wildlife [1,2]. As an essential part of economic development, coastal wetlands host critical natural resources (e.g., oil, gas, salt, and seafood) and provide protective barriers from hazards [3,4]. However, these fragile landscapes are extremely vulnerable and dynamic due to various factors, including global warming, rise in sea level, land subsidence, floods, hurricanes, oil spills, salt-water intrusion, and human activities [1,5]. Therefore, timely mapping and analysis of land degradation and vulnerability is important to prevent land loss and to develop sustainable wetlands [1,6,7].

Land-cover classification based on remotely sensed imagery is a common approach for the analysis of land dynamics. However, users usually need to tailor classification schemes and methods to the specific needs of applications. As a result, many wetland classifications often involve considerable number of land-cover types and a tedious process for sample selection and classification. For example, Sanchez-Hernandez et al. [8] used Support Vector Machine (SVM) method to classify Landsat ETM+ images into eight types of coastal land covers: saltmarsh, fens, agriculture, forest, grazing marsh, sand, urban, and water. Chiu & Couloigner [9] classified Landsat ETM+ (Enhanced Thematic Mapper Plus) data into seven classification types including water body, deciduous forest, wetland, transitions of deciduous forest-wetland, mixed stand, transition of deciduous forest-mixed stand, transition of wetland-mixed stand, and transitions of deciduous forest-wetland-mixed stand. For certain wetland studies, a smaller number of classes may be sufficient such as the four classes (emergent, woody, water and upland) used by Pantaleoni et al. [10] and the three classes (upland, wetland, and intermediate wetland) used by Augusteijn & Warrender [11]. As demonstrated above, the choices of land-cover schemes and names of classes vary greatly with needs from local environments or research teams, and the overall processes become increasingly time consuming with increased classes. On the other hand, notable applications and processes in coastal environments such as land-

loss analysis, barrier island protection, beach nourishment, dune morphology, surface erosion, riverbed or bank stabilization, and wetland conservation share common interests in the interactions among three fundamental elements of soil, water, and the role of vegetation in sediment stabilization [12-15]. Therefore, there is a need for a simplified classification process appropriate for these types of coastal applications.

Existing methods closely related to land dynamics based on land and water include a standard classification method based on sharp land and water contrast in the spectral band of shortwave infrared in Landsat images [16]. This method first identifies land-to-water breaks based on the spectral histograms of land and water in an image, enhances the land-to-water boundary through an edge-enhancement process based on aggregated reflectance values, and then separates land from water based on the selected thresholds. The Louisiana Coastal Area (LCA) Comprehensive Coastwise Ecosystem Restoration Study and the U.S. Geological Survey (USGS) have adopted this method for large-scale land-change mapping [6,16,17]. However, this method may not yield satisfactory results when the boundary between land and water is spectrally vague, particularly due to such water status with high concentration of suspended sediments found in estuary and deltaic coastal environments.

Successful adoption of a simplified strategy in a similar environment indicate the feasibility to develop such a method for coastal applications. In urban environments, Ridd [18] introduced a vegetation-impervious-soil (V-I-S) model in year 1995 to simplify urban land-cover mapping based on three types of land covers: vegetation, impervious area, and soil. The V-I-S model has been widely adopted for urban sprawl and change analysis because of its simplicity and effectiveness [19-21]. Likewise, this research proposes to apply a simplified brightness-greenness-wetness (B-G-W) model for the studies of land dynamics. Exposed land areas with high reflectance such as bare soil, impervious surfaces, and beaches has high Brightness (B) values. Areas covered by vegetation such as grass, marshes, and trees typically have relatively high Greenness (G) values. Water bodies such as oceans, streams, lakes, and ponds have relatively high Wetness (W) values. In fact, the use of similar classes for the Atchafalaya River Basin by Rosen & Xu [22] proved a suitable application of a B-G-W model for coastal-land-dynamics analysis. In their study of land and water dynamics, Rosen & Xu [22] first classified the Atchafalaya Basin in the Mississippi River Delta into twenty-five classes using unsupervised ISODATA classification. They then merged these classes into three wetland classes: barren land, vegetation, and water. Selecting a suitable and simplified method that can fully support the study of land dynamics based on the B-G-W model then becomes necessary.

The goal of this research is to promote the use of simplified B-G-W model for coastal land dynamics analyses and support it through developing an optimal classification approach based on comparative studies of existing strategies. Although various imagery such as MODIS [23,24], ASTER [10], SRTM [24], RADARSAT [25], SPOT [26], WorldView [27], and aerial photographs are applicable for coastal and wetland mapping, Landsat images are still the most commonly used data because of their wide accessibility with free access, suitable spatial resolution for local and regional analysis, and consistent historical archival [4,28,29]. Considering the simplicity of classification scheme, we select SVM classifier based on the proven records of robustness and effectiveness by numerous studies [30-32]. However, uses can adopt other classification methods if necessary. In this research, we focus on the optimal input bands from a combination of original bands and five sets of indices and comparison of pixel- and object-based classifications as well as the adoption of the multi-scale analysis to quantify optimal segmentation scales. The selected approach then formed the base for decadal land dynamics analysis for the Mississippi River bird's-foot delta from 1973 to 2014. Finally, we analyzed the spatial distribution of land loss and land gain and conducted vulnerability analysis based on frequency mapping of land changes.

Materials and Methods

Study site and data

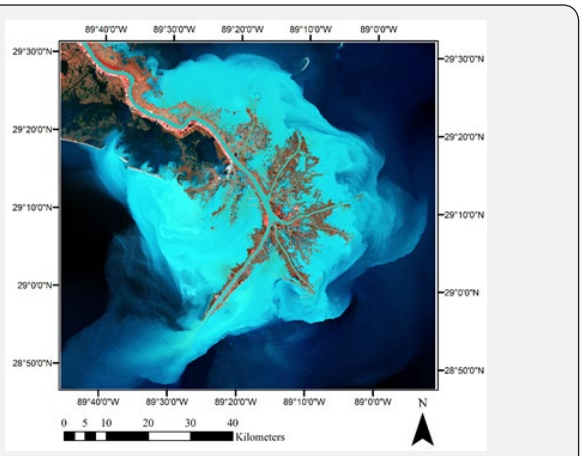

Figure 1: The study site is located in the Mississippi River bird's-foot delta. The extent is illustrated in the Landsat 8 image downloaded in 2014 from the USGS website and illustrated in color infrared composed of Bands 3, 4, and 5.

The study site is located in the bird's-foot delta of the Mississippi River in the state of Louisiana, and the test images covers an area of 10.3km^2 as shown in Figure 1. The Mississippi River is the seventh largest river in the world and contains a large watershed network flowing from the north to the south of the U.S. and enters the Gulf of Mexico through the bird's-foot delta and the Atchafalaya River [33]. Sitting in the flood plain of the Mississippi River, Louisiana possesses forty percent of the wetlands of the United States, which provide rich oil and gas resources, habitats for fishery and wildlife, and coastal shoreline protection [34,35]. However, these wetlands are suffering from an alarming rate of land loss in recent decades [35]. Land degradation and vulnerability are critical issues for wetland conservation.

How to cite this article: Xuelian M, Haitian Z. Coastal Land Dynamics and Vulnerability Analyses based on the Brightness-Greenness-Wetness Model. Int J Environ Sci Nat Res. 2019; 22(5): 556098. DOI: 10.19080/IJESNR.2019.22.556098

Land cover features at the study site mainly include marshes, trees, barrier islands, water channels, and man-made structures. Human settlements and commercial structures dominant the narrow linear zone along the elevated levees. To analyze the land dynamics, this research first selected an optimal classification method based on the B-G-W model through a classification comparison based on the image taken in 2013 and then applied the selected method for decadal land dynamics analysis for the years of 1973, 1983, 1994, 2003, and 2014. Table 1 lists images, water level source, and hurricane information for the study site. One important consideration for quality control is to minimize impacts from external factors such as seasonal variations of vegetation status, weather (e.g. floods and cold fronts), water level, intervals between images, and cloud coverage. Due to frequent presents of heavy clouds in coastal environment, cloud-free Landsat images for the delta front are mostly available in October and January in some years. Therefore, this research selected cloud-free images in the winter season (January) with low water levels in consistent months and over a decadal interval [22]. Cloud-free images with consistent seasons were not available for denser interval of years.

Table 1: Description of data used in this research.

Data Category	Date	Sensor	Resolution used for Classification	Source
Landsat imagery	1/16/1973	Landsat 1	60m	USGS http://earthexploer.usgs.gov/
	1/15/1983	Landsat 4 TM	30m	
	1/21/1994	Landsat 5 TM	30m	
	1/14/2003	Landsat 5 TM	30m	
	10/24/2013	Landsat 8	30m	
	1/12/2014	Landsat 8	30m	
Water level	1973	Water gate	Monthly average and minimum Hourly	NOAA tides and currents records at Grand Isle Island
	1983-2014	Water gate		
Hurricanes and storm surges	Memorable Gulf Coast hurricanes of the 20th century			NOAA
	List of Louisiana hurricanes (2000–present)			Wikipedia

This research used atmospherically corrected data for the years 1983, 1994, and 2003 from the Landsat CDR Program and conducted atmospheric correction for new images in 2013 and 2014 using the FLAASH method in ENVI software. Due to the limited number of bands for Landsat 1 images, the challenges in conducting atmospheric correction, and the limited impact of atmospheric classification on qualitative classification, data process for the image in 1973 used the original image and resample it to 30-meter-resolution to be consistent with the other images. These Landsat images are in Universal Transverse Mercator (UTM) projection, Zone 16 N, Datum WGS 1984.

Selection of classification method to support analysis of land dynamics based on the B-G-W model

SVM classification algorithm

The SVM classifier in remote sensing is a non-parametric, supervised classification algorithm based on machine learning [31]. This research selects SVM for classification because of its proven robustness and reliability by many studies [30,36]. The algorithm finds hyperplanes to separate a given data set into different predefined classes. In a simplified scenario to separate two classes, SVM finds an optimal decision hyperplane with the widest region of separation defined by two parallel hyperplanes passing through the edges of class clusters from training samples [2]. Support vectors are the samples located on the parallel hyperplanes. Since many real world classification scenarios may not be linearly separable, the method extends the linear decision hyperplane to a non-linear one by adding a penalty parameter, a slack value to the distance constrain, and the use of kernel functions [2]. SVM algorithm further extend the two-class classification to a multi-class classification through one-against-one or one-against-all strategies [31]. The multi-class SVM classification used in this research uses the Library for Support Vector Machines (LIBSVM) developed by Chang & Lin [37] for the open source data mining software of Weka (Waikato Environment for Knowledge Analysis) [2] and is available in ENVI software for wider applications.

The SVM classification method gains its popularity through reliable classification accuracy and easy implementation [30]. However, to achieve its best performance, making a choice among multiple combinations between parameters and options of various kernel functions often overwhelms users [2]. Popular kernel functions mainly include four types of functions (linear, polynomial, sigmoid, and radial basis function [RBF]), among which polynomial and RBF kernels are relatively popular [2]. This research select a RBF kernel that requires a priori tuning of the kernel width (γ) and penalty parameter (C) through an optimization process called grid search in Weka [2,31]. For a thorough explanation of SVM and kernel functions, please see Kavzoglu & Colkesen [2]. Mountrakis, Im & Ogole [30] provided a general review of SVM application in the field of remote sensing.

How to cite this article: Xuelian M, Haitian Z. Coastal Land Dynamics and Vulnerability Analyses based on the Brightness-Greenness-Wetness Model. Int J Environ Sci Nat Res. 2019; 22(5): 556098. DOI: 10.19080/IJESNR.2019.22.556098

Multi-scale analysis for optimal segmentation scale

The initial step in object-based classification is to generate objects through segmentation or classification methods to group adjacent pixels with similar values into objects [38,39]. Different parameters applied in the segmentation procedure will generate objects with different scales in correspondence to variation of object size and heterogeneity. For example, a segmentation scale with higher heterogeneity generates bigger objects with pixels of larger value differences. As a result, selection of segmentation scales is often through trial and error approach and has a significant impact on the accuracy of the object-based classification. In 2011, a multi-scale analysis for unsupervised segmentation introduced the concept of a global score (GS) to evaluate the goodness of segmentation based on normalized weighted variance (Vnorm) and Moran's I (MInorm) [38]. The scale with the lowest GS value indicates the optimal scale for segmentation. This research applied this multi-scale analysis to the selected Landsat images to identify the optimal scale for object-based classification and then selected the training and assessment samples based on these segmentation results.

Comparison of pixel- and object-based classification and accuracy assessment

Pixel- and object-based classifications work on different kinds of units (e.g., a pixel vs. an object of connected pixels), which raises a challenge for comparative studies. This research applied two main strategies to allow supervised training and accuracy assessment of pixel- and object-based classification results through comparable samples in corresponding locations. First, the multi-scale analysis described in the previous section used unsupervised segmentation to form object boundaries at the optimal scale. Second, the object-based classification method used a set of randomly selected samples for training and assessment, while the pixel-based method classified images based on the pixels located at the corresponding centers of the objects. However, these corresponding center pixels could be in arbitrary locations that were difficult to identify land cover classes. To ensure fair evaluation of pixel- and object--based methods, these pixel samples were adjusted to adjacent locations in correspondence to the object type when necessary [40]. Finally, quantitative accuracy assessments compared performance based on overall accuracy and kappa value, which is a common approach in remote sensing for classification comparison. The overall accuracy is the total number of accurately classified samples divided by the total number of samples without considering the classification accuracy of individual classes. As a result, overall accuracy may still be high even some classes have low accuracies. To compensate this limit, users often report kappa coefficient value calculated from the confusion matrix where individual classes with poor accuracy will have a significant impact on the kappa value. Congalton & Green [41] gave a detailed introduction about these accuracy assessment methods in remote sensing.

Decadal land dynamics analysis for fragmented coastal wetlands

For dynamic analysis of fragile and fragmented coastal lands, classification accuracies may have a significant impact on perception of land dynamics, especially for the under-represented classes (e.g., soil in this research). Since the main components of land and water dynamics are soil, vegetation, and water in corresponding to the B-G-W model, the use of related indices may be a suitable and necessary approach to improving classification accuracy. For land-cover classification based on Landsat imagery, the most commonly used bands are the original or atmospherically corrected bands with digital numbers (DN). Other potential useful bands are indices related to vegetation, soil, and water (referred to as the three indices from here, as defined below) and the indices derived from KTC transformation [42].

In order to evaluate the optimal input bands for coastal land dynamics studies based on the B-G-W model, this research conducted pixel- and object-based classification with these three types of inputs: Landsat bands (referred to as DN), the three indices, and the KTC-transformed indices. The three indices used in this research are Normalized Difference Vegetation Index (NDVI), Normalized Difference Built-up Index (NDBI), and Normalized Difference Water Index (NDWI). Developed by Rouse et al. [43] and widely used for vegetation mapping and land cover classification, NDVI calculates vegetation index using the near-infrared (NIR) and red bands as illustrated in Equation (1). Zha et al. [44] presented an NDBI index for mapping urban-extent based on Landsat imagery as in Equation (2), which is sensitive to land overs with high reflectance such as soil, beach and roads. For NDWI, there are three variations as introduced by Xu [45]: NDWI, modified NDWI (MNDWI), and NDWIGAO. McFeeters [46] introduced the NDWI index using the green and NIR bands as expressed in Equation (3). Replacing the NIR band with the MIR band, Xu [45] modified this water index to the MNDWI using Equation (4), claiming reduction of noises from built-up land. NDWIGAO was developed by Gao [47] with a form similar to the NDBI index. Therefore, this research compared NDWI and MNDWI indices for the analysis of coastal land dynamics. Kauth et al. [48] developed the KTC transformation for Landsat MSS (Multispectral Scanner System) imagery to remove redundant information with high correlations and generate a new set of transformed indices of brightness, greenness, yellow stuff, and non-such. Crist & Kauth [49] then modified the indices for Landsat TM imagery as brightness, greenness, and wetness as illustrated in the following Equations (5)-(7). Since Landsat 8 imagery has spectrum ranges similar to Landsat 5 imagery, the same equations are applicable to the images acquired in 2013 and 2014 by replacing the band number with Bands 2, 3, 4, 5, 6, 7 in the corresponding order.

How to cite this article: Xuelian M, Haitian Z. Coastal Land Dynamics and Vulnerability Analyses based on the Brightness-Greenness-Wetness Model. Int J Environ Sci Nat Res. 2019; 22(5): 556098. DOI: 10.19080/IJESNR.2019.22.556098

$$NDVI = \frac{NIR - \mathrm{Re}d}{NIR + \mathrm{Re}d} \quad (1)$$

$$NDBI = \frac{MidIR - NIR}{MidIR + NIR} \quad (2)$$

$$NDWI = \frac{Green - NIR}{Green + NIR} \quad (3)$$

$$MNDWI = \frac{Green - MIR}{Green + MIR} \quad (4)$$

$$B = 0.2909\ TM1 + 0.2493\ TM2 + 0.4806\ TM3 + 0.5568\ TM4 + 0.4438\ TM5 + 0.1706\ TM7 \quad (5)$$

$$G = -0.2728\ TM1 - 0.2174\ TM2 - 0.5508\ TM3 + 0.7221\ TM4 + 0.0733\ TM5 - 0.1648\ TM7 \quad (6)$$

$$W = 0.1446\ TM1 + 0.1761\ TM2 + 0.3322\ TM3 + 0.3396\ TM4 - 0.6210\ TM5 - 0.4186\ TM7 \quad (7)$$

Results

Data preprocessing and classification comparison

Data preprocessing, segmentation scale analyzing, and data sampling

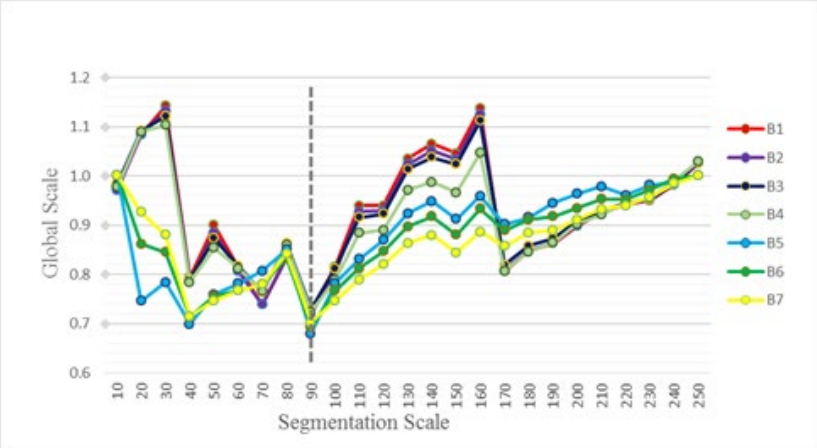

Figure 2: The results of multi-scale analysis for the Landsat image acquired on October 24, 2013. This analysis used atmospherically corrected bands (B1-B7) with a spatial resolution of 30 meter. The lowest global scale value in each band is located at the scale of 90, indicating the best scale for object segmentation.

Table 2: Statistics of training and accuracy assessment samples used in pixel- and object-based classification comparison. The units are number of samples.

Class	Training Samples	Assessment Samples	Total Count
Soil	50	50	100
Vegetation	58	58	116
Water	124	123	247
Total Count	232	231	463

The bands used for land-cover analyses include four original bands of the 1973 image along with atmospherically corrected Bands 1-5 and 7 of Landsat TM images and Bands 1-7 and 9 for Landsat 8 images. For a comparative study based on the 2013 imagery, a multi-scale analysis based on multi-resolution segmentation first quantified the optimal segmentation scale based on the selected inputs (Figure 2). As adding panchromatic band with a higher resolution did not generate the lowest GS values at unified scale, classification process excluded panchromatic bands from input options. The segmentation scale in the horizontal axis is a unit-free parameter that will influence the size and heterogeneity of the derived objects [38]. In this study site, the scale of 90 generated the lowest GS score in each band and functioned as the parameter for the following object-

How to cite this article: Xuelian M, Haitian Z. Coastal Land Dynamics and Vulnerability Analyses based on the Brightness-Greenness-Wetness Model. Int J Environ Sci Nat Res. 2019; 22(5): 556098. DOI: 10.19080/IJESNR.2019.22.556098

based classification. From 6688 polygons, this research randomly selected approximately 10% of these polygons for training and accuracy assessment and used their corresponding pixels located in the geometric centers or adjacent pixels in the corresponding classes for pixel-based classification. As a result, this research used 232 pixels for training and 231 samples for accuracy assessment as illustrated in Table 2.

Table 3: Comparison of pixel- and object-based SVM classification results and their parameters from grid search based on Landsat images taken on October 24, 2013.

Category	Input Bands	Cost, Kernel Width	Overall Accuracy	Kappa
Object	DN	222.0, 2-18.0	93.36%	0.8938
	KTC	27.0, 2-23.0	95.67%	0.929
	Three indices with MNDWI	23.0,25.0	95.02%	0.9203
	Three indices with NDWI	223.0,25.0	95.44%	0.9268
Pixel	DN	26.0, 2-20.0	93.07%	0.8871
	KTC	24.0,2-20.0	95.85%	0.9333
	Three indices with MNDWI	220.0, 24.0	96.10%	0.9335
	Three indices with NDWI	220.0, 25.0	93.94%	0.8947

Comparison of pixel- and object-based land-cover classification

This section compares pixel- and object-based classification using the SVM method with the RBF kernel function as illustrated in Table 3. For each classification experiment, a grid search method in Weka software determined the best parameters of cost and kernel width for the SVM method within a given search range through a cross-validation approach. Supposing there are n training samples, the cross-validation approach takes out one training sample for accuracy assessment and runs the SVM classification based on the remaining n-1 samples. Then the process throws that removed sample back into the training pool, selects a new sample, and conducts another classification until taking out every point once. As a result, there are a total number of n samples for accuracy assessment. This cross-validation approach can reduce the possibility of over-fitting and is especially useful for applications with a limited number of training samples, which is ideal for the fragmented coastal land-cover analysis in this research. The use of a grid search range for the exponent (as illustrated in Table 3) of the cost and kernel width optimizes search efficiency. Hsu et al. [50] selected a range of -5 to 15 for SVM based on the RBF kernel. This research used a range of -20 to 20 with a maximum number of grid extensions of 3. Please refer to [2,50] for a detailed description of the kernel functions and parameters. Table 3 presents the best parameters for cost and kernel width based on the grid search results and the overall accuracy and kappa values for the pixel- and object-based SVM classification with different inputs.

The comparative results in Table 3 shows that the use of KTC or three indices with MNDWI does improve overall accuracy around 2-3 percent in comparison to the results based on Landsat reflectance in DN. The highest accuracy appears to be the pixel-based SVM classification based on the three indices with MNDWI. However, some obvious confusion between brightness and wetness occurred in areas in open water as inherited from the DNBI index. As the results based on KTC were more consistent and reliable and pixel-based classification provides comparable classification accuracy based on kappa value with a much simpler procedure, the pixel-based SVM classification based on KTC transformation was more preferable for the decadal land dynamics analysis in the Mississippi River bird's-foot delta.

Decadal land dynamics analysis at the bird's-foot delta

Decadal land-cover dynamics and statistics

Table 4: The grid search results and classification accuracy for decadal land classification in the Mississippi River bird's-foot delta.

Year	Input Bands	Cost, Kernel Width	Overall Accuracy	Kappa
1/16/1973	DN	223, 2-13	99.08%	0.99
1/15/1983	KT	223, 2-18	99.57%	0.89
1/21/1994	KT	223,2-20	98.27%	0.93
1/14/2003	KT	221, 2-19	99.13%	0.93
1/12/2014	KT	223, 2-19	95.67%	0.89

For decadal land dynamics analysis, this research conducted pixel-based SVM classification method validated in the above comparative session on images in 1973, 1983, 1994, 2003, and 2014 based on KTC transformation. The two sets of training and

How to cite this article: Xuelian M, Haitian Z. Coastal Land Dynamics and Vulnerability Analyses based on the Brightness-Greenness-Wetness Model. Int J Environ Sci Nat Res. 2019; 22(5): 556098. DOI: 10.19080/IJESNR.2019.22.556098

assessment sample locations for the 2013 image were applied to decadal images with their land-cover types verified from the corresponding images. Table 4 lists the grid search results with the best parameters for SVM classification and the overall accuracies and kappa values for the decadal land classification based on the B-G-W model. The classification results demonstrated overall accuracies over 95%, indicating reliable classification results for decadal land change analysis. Table 5 shows area statistics of land cover types in each year, and Figure 3 illustrates the spatial distribution of land cover types.

Table 5: Decadal land-cover statistics at the bird's-foot delta from 1973 to 2014. The units are km^2.

Year	Brightness	Vegetation	Brightness + Vegetation	Wetness
1973	28.93	859.17	888.1	6426.86
1983	26.7	576.15	602.85	6712.1
1994	49.54	792.58	842.12	6472.84
2003	14.5	677.48	691.99	6622.97
2014	24.13	605.74	629.87	6685.08

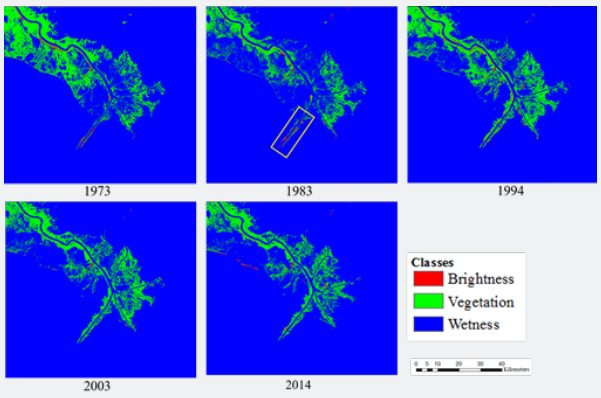

Figure 3: The decadal land-cover classification results in the Mississippi River bird's-foot delta. The area outlined in the box represents bare soil (brightness) followed by vegetation colonization since the year of 1994.

The decadal land classification results in Figure 3 and table 5 indicate the following observations.

a) The total land areas (brightness + vegetation) correlate highly with the vegetated areas. This means that bare lands rarely survive without vegetation cover, and vegetation plays a vital role in sediment stabilization in a fragile coastal environment frequently influenced by river discharge, windstorms, and hurricanes.

b) As a minority class, brightness was mainly at three types of locations: beaches on barrier islands, levees, and sediment deposit at the mouths of river discharges. Since colonization of vegetation often follows sediment deposition to stabilize sediment, the locations of emerging soil or beaches often indicate areas of early land growth. A particular example in Figure 3 as outlined in the yellow box demonstrates that a notable area of soil located in the southwest river outlet present in the 1973 and 1983 images was later stabilized by vegetation as seen in the 1994, 2003, and 2014 images.

c) Small yet concentrated soil patches appear in the images from 2014 showing human activities of sand berm construction for wetland restoration. In the recent decade, the alarming rate of land loss at the bird's-foot delta has gained state and federal attention for coastal shoreline protection. The state of Louisiana conducted sand berm construction at four barrier islands (Pelican, Shell, Scofield, and Chandeleur Islands) in 2012 with funds from the 2010 BP oil spill. Some of these constructed sand berms disappeared quickly due to tides and waves and needed periodical nourishment. The outlined box 1 in Figure 4 shows the recent status in January 2014. The areas outlined in boxes 2 and 3 in Figure 4 are reconstructed sand berms occurred more recently.

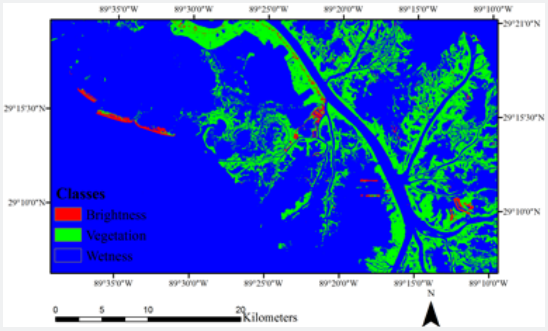

Figure 4: A zoomed-in view of the newly constructed sand berms appeared in the classification results of 2014 as highlighted in the yellow boxes.

Spatial distribution analysis of land loss, land gain, and stable land

Coastal land loss is a major concern as nearly a third of the human population live in the coastal zones [51]. By combining vegetation and brightness classes into one land class, Figure 5 provides decadal land dynamics map based on land and water. The results showed that the bird's-foot delta had been experiencing an overall trend of land loss as demonstrated in Table 5 and Figure 5. The land in 1983 had the most significant loss rate of 32.12% comparing to 1973. Although land in 1994 showed area increase comparing to 1983 but was still a 5.2% loss comparing to 1973. Significant and permanent land loss occurred at the upper river stream at the southwest side of the levee (areas include Barataria Bay, Bastian Bay, Adam Bay, Bay Pomme d'or, and Bay Jacques),

How to cite this article: Xuelian M, Haitian Z. Coastal Land Dynamics and Vulnerability Analyses based on the Brightness-Greenness-Wetness Model. Int J Environ Sci Nat Res. 2019; 22(5): 556098. DOI: 10.19080/IJESNR.2019.22.556098

with the major land loss occurring between 1973 and 1983. This permanent land loss had been witnessed and confirmed by local fishermen at Buras, Louisiana, where nearby wetlands showed as large open water. Land change analysis by Barras et al. [16] confirmed major land loss in this area between 1978-1990 and scattered patches of land loss in the following decade. One of the major events occurring right before this examined time frame was the intensive construction of levees and guided drainage systems in the Barataria Bay and Breton Sound Basins between 1940 and 1970 [52]. This construction significantly reduced sediment deposition in the area with a combined effect of land subsidence from compaction of the soft sedimentary layers. Consequently, in early 1980s the U.S. Army Corps of Engineers [52] reported significant saltwater intrusion in the Barataria Bay and Breton Sound Basins that resulted in killing freshwater marshes in the area and permanently convert the marshes to open water.

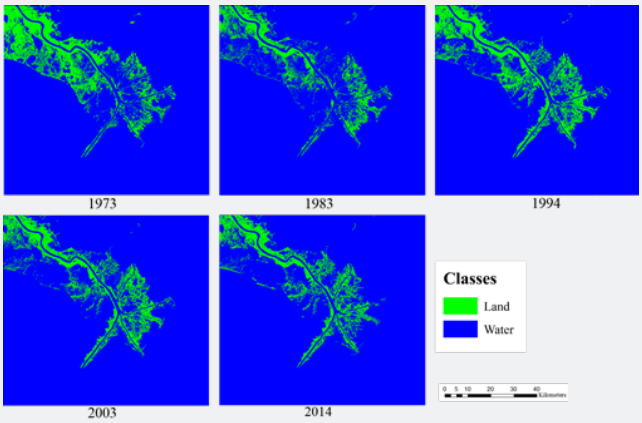

Figure 5: The decadal land distribution in the Mississippi River bird's-foot delta by combining vegetation and brightness classes into land.

As one of the major driven factors of saltwater intrusion, the natural hazards of hurricanes further contributed to this land loss [16,53]. The major hurricane events occurred in the Gulf Coast between 1983 and 1994 and between 1994 and 20014 are listed in Table 6 for comparison [54]. Hurricane Frederic occurred on September 13, 1979 with a wind power up to 145mph. Hurricane Allen, which occurred on August 9-10, 1980, was a Category 5 (the strongest level recorded) event [55]. The land changes between 2003 and 2014 in Figure 6 showed a concentrated area of land loss along the northeast river outlets. A likely cause for this could be frequent and intense hurricanes and the resulted salt-water intrusion. When compared to other periods, this recent decade had the highest number of hurricanes including the well-known destructive Hurricane Katrina [54,55]. Nine hurricanes occurred in these ten years as listed in Table 6. Among these hurricanes, Hurricane Katrina caused the most destructive flood event in the city of New Orleans in 2005. Katrina was a high Category 5 and then dropped to Category 3 when it moved inland. Numerous studies have reported severe land loss in coastal Louisiana due to Hurricane Katrina [56,57]. The associations between major hurricane events and the severe levels of land losses indicate the significant impact of hurricanes on coastal land dynamics. The results demonstrate that the classification results based on B-G-W model can directly support the analysis of land dynamics.

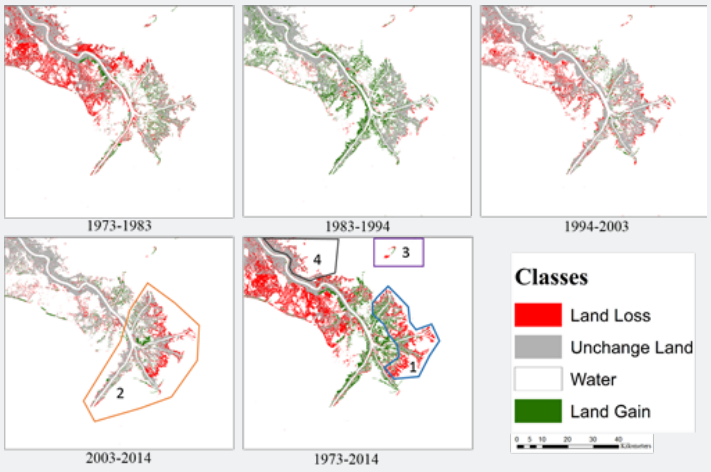

Figure 6: The decadal land change analysis in terms of stable land, water, land loss, and land gain.

How to cite this article: Xuelian M, Haitian Z. Coastal Land Dynamics and Vulnerability Analyses based on the Brightness-Greenness-Wetness Model. Int J Environ Sci Nat Res. 2019; 22(5): 556098. DOI: 10.19080/IJESNR.2019.22.556098

Table 6: List of major hurricane events from the year of 1973 to 2014 based on historical records.

Period	Hurricane	Time
1973-1983	Carmen	August 29-September 10, 1974
	Bob	July 9-16, 1979
	Frederic	September 13, 1979
	Allen	August 9-10, 1980
1983-1994	Alicia	August 18, 1983
	Danny	August 12-18, 1985
	Elena	September 2, 1985
	Juan	October 26-November 1, 1985
	Bonnie	June 23-28, 1986
	Florence	September 7-11, 1988
	Gilbert	September 16, 1988
	Andrew	August 26, 1992
1994-2003	Danny	July 16, 1997
	Isidore	September 26, 2002
	Lili	October 2, 2002
2003-2014	Ivan	September 23, 2004
	Cindy	July 5, 2005
	Dennis	July 10, 2005
	Katrina	August 29, 2005
	Rita	September 24, 2005
	Humberto	September 13, 2007
	Gustav	August 31, 2008
	Ida	November 10, 2009
	Isaac	August 29, 2012

To further analyze spatial distribution pattern of land dynamics, Figure 6 demonstrates the decadal land changes with grey color representing stable (unchanged) land, red representing areas of land loss, and green representing areas of land gain. These results showed uneven distribution of land change characteristics. In contrast to the significant land loss in the southwest side of the river levee as discussed in previous sections, significant land loss at the outskirts of the river outlets as outlined in the box 1 in Figure 6; however, obvious land gain occurred along the beginning portion of the river outlets where sediment deposit started. In addition, comparing to the main outlets in box 2, the outlets on the west side of the river are relatively stable than the outlets on the east side of the Mississippi River. The Breton Island further east are fading away and will likely disappear in few more decades if current trend continues. However, the wetland in northeast outlined in box 4 in Breton Sound is relatively stable in the past four decades. The land area along the main Mississippi River is most stable likely because of the protection of elevated terrain.

Human activities such as fishing and dredging have no doubt played a significant role in the bird's-foot delta. Morton and Barras [53] reported that the digging of trenches and navigational channels, modification of surface elevations in marshes, and disturbed wetland morphology could promote the formation of ponds and increase the degree of wetland fragmentation. Levee construction, river diversion controls, and water consumption in the upper stream of the river have significantly affected sediment discharge to the lower Mississippi River [5,24,58]. In addition, extensive discharge from agricultural fields has caused dead zones in the Gulf of Mexico due to a lack of oxygen, which has significantly altered habitat environment and accelerated land degradation [59].

Land-cover change frequency mapping for assessment of the level of land dynamics and vulnerability

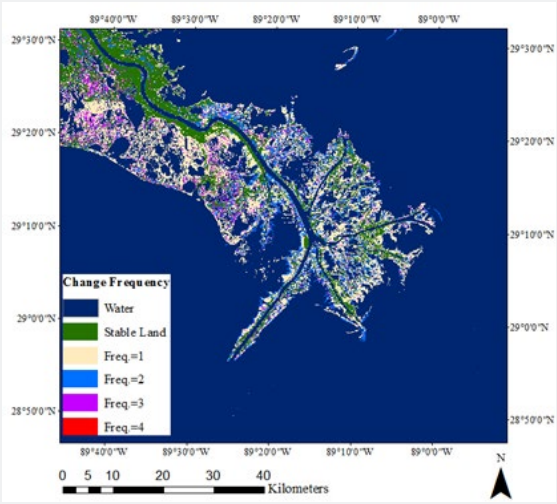

Figure 7: Map of land change frequencies in the Mississippi River bird's-foot delta.

The decadal land-cover mapping results in the previous section demonstrates land-cover status in ten-year intervals. This research presented an approach to the mapping of land-cover change frequency and applied the analysis for land vulnerability analysis. How frequently the land changes over time indicates a certain level of land dynamics in the area and provides valuable insights into land vulnerability and their spatial distribution patterns. Figure 7 is the result of land-cover change frequency mapping by counting the number of land-cover changes. For example, if a class changes from land to water, the time of change is 1. If the class changes again in the next decade, then the number is summed up to 2. The derived frequencies in this research

How to cite this article: Xuelian M, Haitian Z. Coastal Land Dynamics and Vulnerability Analyses based on the Brightness-Greenness-Wetness Model. Int J Environ Sci Nat Res. 2019; 22(5): 556098. DOI: 10.19080/IJESNR.2019.22.556098

ranges from 0 to 4 as a total of 5 temporal images used. For the unchanged areas (frequency equal to 0), water is colored deep navy blue and land is colored a deep green. The areas changing at least one time are in colors as noted in the legend in Figure 7.

The stable land areas (deep green color in Figure 7) represent the land unchanged over the past four decades. Therefore, government officials can optimize wetland conservation by directing more resources to other vulnerable areas with more land growth potential. Relatively fewer areas changed in all four periods (red), but areas changing two to three times existed widely in the study site, especially at the southwest region and along river outlets. The interpretation of this category may vary the sequences of the changes. When frequent changes occurred in early stages and remain unchanged in the later stage of the periods, this scenario might indicate permanent changes to the end land-cover type. If lands remain stable in early stages and change frequently in recent decades, the areas tended to be relatively vulnerable but might have the potential to change back to land as past changes had demonstrated such potential. Similarly, one time of land-to-water change occurred in an early period meant permanent land loss due to no sign of recovery in recent decades, indicating the most vulnerable areas in the Mississippi River bird's-foot delta in the past four decades. This was particularly evident in the upper areas to the southwest of levees. This mapping of land change frequency provides quantitative physical evidence regarding the times of land changes over the selected periods and temporal intervals.

Discussion

This research compared the pixel- and object-based approaches in order to find the optimal method to support the use of B-G-W model for coastal land dynamics analysis. Determining segmentation scale is often a critical and challenging issue traditionally solved by a trial and error approach. This research experimented the unsupervised multi-scale segmentation analysis method developed in 2011 [38] and proved its effectiveness to determine the optimal scale parameter through the quantitative statistics of global score. Adding panchromatic image to the multi-scale analysis resulted in disagreement of the lowest GS scores at different bands, suggesting a negative impact and exclusion from the multi-scale analysis.

Comparison between the pixel- and object-based methods is a common topic when selecting proper approach for land-cover classification. Since multiple studies have demonstrate the superior performance of object-based land-cover classification over pixel-based methods, one is likely to assume that object-based methods perform better in most applications. However, for fragmented coastal wetlands, object-based methods do not necessarily generate better results for simplified B-G-W model. In fact, equal amounts (two out of the four input options) of best performance existed in pixel- and object-based classifications in this research when using the same input bands. Considering the challenges in determining a suitable scale and other parameters, the object-based land-cover classification approach is more complicated to implement comparing to the pixel-based methods. The results showed that the supervised-classification based on SVM and KTC transformed indices provide a robust and reliable result to support the B-G-W model-based land dynamics analyses. This method is easy to understand and implement as commonly used software such as ENVI support both SVM and KTC transformation. Users have the flexibility to opt to use other classification methods or input data if necessary.

The extended decadal land change analysis demonstrated the convenient use of the proposed method to support land dynamics analysis and quantification of land vulnerability. When applying this tool for vulnerability analysis, the meaning of the change frequencies may vary with the sequences of land changes. Increasing the temporal scale (such as from ten years to five or even one year) can significantly increase the reliable interpretation of land dynamics. However, clouds-free Landsat images with consistent season and smaller year intervals are not available for this study site, which prohibits the test of higher temporal scale in this research.

Conclusion

Fragmented landscapes in coastal and wetland areas are often results of frequent disturbances from weather events and hydrological processes. This research adopted a simplified B-G-W model for coastal land dynamics mapping and vulnerability analysis based on decadal land changes. To seek optimal mapping solution based on the SVM classifier, a comparative study evaluated various combinations of input bands and pixel- vs. object-based classification methods. When compared to object-based classification, the results indicate that pixel-based classification provides a reliable yet simpler classification approach for fragmented coastal landscapes based on B-G-W model. We compared three types of bands for classification: Landsat DN bands, KTC-transformed brightness, greenness, and wetness, and three indices of water, soil, and vegetation. Although the derived accuracies were compatible, the results based on KTC provided the most reliable and consistent performance. As a result, our comparative study indicated that the best approach was a pixel-based SVM classification through KTC transformation and B-G-W model.

This research further validated and applied the method for decadal land change analysis and vulnerability assessment in the Mississippi River bird's-foot delta. The results of decadal land dynamic analysis showed significant land loss in the southwest area near Barataria Bay and sediment deposit along major river outlets. Especially, the southwest outlet of the Mississippi River demonstrated a typical coastal land building process where vegetation colonization followed some early land development. In addition, three locations of sand berm reconstructions showed up in the 2014 classification results. Combing brightness and

How to cite this article: Xuelian M, Haitian Z. Coastal Land Dynamics and Vulnerability Analyses based on the Brightness-Greenness-Wetness Model. Int J Environ Sci Nat Res. 2019; 22(5): 556098. DOI: 10.19080/IJESNR.2019.22.556098

vegetation into one land class can conveniently support land vs. water dynamics analysis based on stable land, land loss and land gain. Results provide valuable planning support for coastal land conservation. Finally, this research presented a method for mapping land change frequency to indicate the intensity of land dynamics and vulnerability. This change frequency provides three main information: areas with stable land for lesser efforts in land conservation; most vulnerable areas with either frequent land changes or low land change frequency yet nonreversible changes; and areas with wide distribution and moderate land changes representing the best candidates for land conservation as their past records demonstrated land growth potential. Overall, this research demonstrates the simplicity and effectiveness of the B-G-W model for coastal land dynamics and vulnerability analysis.

Acknowledgment

This research is supported by the Louisiana State University through Summer Stipend Program of the Office of Research & Economic Development, and start-up fund of the College of Humanities & Social Sciences. The authors would like to thank the anonymous reviewers for their valuable comments.

Author Contributions

Xuelian Meng contributed to the over design of research and leaded the writing of the manuscript. Haitian Zhu contributed to data processing, spatial analysis, and manuscript writing.

References

1. Coleman JM, Roberts HH, Stone GW (1998) Mississippi river delta: An overview. Journal of Coastal Research 14(3): 698-716.
2. Kavzoglu T, Colkesen I (2009) A kernel functions analysis for support vector machines for land cover classification. Int J Appl Earth Obs Geoinf 11(5): 352-359.
3. Klemas V (2013) Remote sensing of emergent and submerged wetlands: An overview. Int J Remote Sens 34(18): 6286-6320.
4. Han X, Chen X, Feng L (2015) Four decades of winter wetland changes in poyang lake based on landsat observations between 1973 and 2013. Remote Sens Environ 156: 426-437.
5. Syvitski JPM, Kettner AJ, Overeem I, Hutton EWH, Hannon MT, et al. (2009) Sinking deltas due to human activities. Nat Geosci 2: 681-686.
6. Couvillion BR, Barras JA, Steyer GD, Sleavin W, Fischer M, et al. (2011) Land area change in coastal louisiana from 1932 to 2010. U.S. Geological Survey Scientific Investigations Map, 3164, scale 1:265,000, p. 12.
7. Coleman JM (1988) Dynamic changes and processes in the Mississippi river delta. Geol Soc Am Bull 100: 999-1015.
8. Sanchez-Hernandez C, Boyd DS, Foody GM (2007) Mapping specific habitats from remotely sensed imagery: Support vector machine and support vector data description based classification of coastal saltmarsh habitats. Ecological Informatics 2(2): 83-88.
9. Chiu WY, Couloigner I (2006) Modified fuzzy c-means classification technique for mapping vague wetlands using landsat etm plus imagery. Hydrol Process 20(17): 3623-3634.
10. Pantaleoni E, Wynne RH, Galbraith JM, Campbell JB (2009) Mapping wetlands using aster data: A comparison between classification trees and logistic regression. Int J Remote Sens 30(13): 3423-3440.
11. Augusteijn MF, Warrender CE (1998) Wetland classification using optical and radar data and neural network classification. Int J Remote Sens 19(8): 1545-1560.
12. White DA (1993) Vascular plant community development on mudflats in the Mississippi river delta, Louisiana, USA. Aquat Bot 45: 171-194.
13. Sasser CE, Gosselink JG, Swenson EM, Swarzenski CM, Leibowitz NC (1996) Vegetation, substrate and hydrology in floating marshes in the mississippi river delta plain wetlands, USA. Vegetatio 122(2): 129-142.
14. Rejmanek M, Sasser CE, Gosselink JG (1987) Modeling of vegetation dynamics in the Mississippi river deltaic plain. Vegetatio 69(1-3): 133-140.
15. De Asis AM, Omasa K (2007) Estimation of vegetation parameter for modeling soil erosion using linear spectral mixture analysis of landsat etm data. ISPRS J Photogramm Remote Sens 62(4): 309-324.
16. Barras J Beville S, Britsch D, Hartley S, Hawes S, et al. (2003) Historical and projected coastal Louisiana land changes—1978–2050. Appendix B of Louisiana Coastal Area (LCA), Louisiana Ecosystem Restoration Study: U.S. Geological Survey Open-File Report 2003-334, p. 39.
17. Morton RA, Bernier JC, Barras JA, Ferina NF (2005) Rapid subsidence and historical wetland loss in the Mississippi delta plain: Likely causes and future implications. U.S. Geological Survey Open-File Report 2005-1216, p. 124.
18. Ridd MK (1995) Exploring a v-i-s (vegetation -impervious surface-soil) model for urban ecosystem analysis through remote sensing - camparative anatomy for cities. Int J Remote Sens 16: 2165-2185.
19. Phinn S, Stanford M, Scarth P, Murray AT, Shyy PT (2002) Monitoring the composition of urban environments based on the vegetation-impervious surface-soil (vis) model by subpixel analysis techniques. Int J Remote Sens 23(20): 4131-4153.
20. Hung M, Ridd MKA (2002) subpixel classifier for urban land-cover mapping based on a maximum-likelihood approach and expert system rules. Photogrammetric Engineering & Remote Sensing 68: 1173-1180.
21. Lu D, Weng Q (2006) Use of impervious surface in urban land-use classification. Remote Sens Environ 102(1-2): 146-160.
22. Rosen T, Xu YJ (2013) Recent decadal growth of the atchafalaya river delta complex: Effects of variable riverine sediment input and vegetation succession. Geomorphology 194: 108-120.
23. Michishita R, Gong P, Xu B (2012) Spectral mixture analysis for bi-sensor wetland mapping using landsat tm and terra modis data. Int J Remote Sens 33(11): 3373-3401.
24. Syvitski JPM, Overeem I, Brakenridge GR, Hannon M (2012) Floods, floodplains, delta plains - a satellite imaging approach. Sedimentary Geology 267-268: 1-14.
25. Rio JNR, Lozano-Garcia DF (2000) Spatial filtering of radar data (radarsat) for wetlands (brackish marshes) classification. Remote Sens Environ 73(2): 143-151.
26. Davranche A, Lefebvre G, Poulin B (2010) Wetland monitoring using classification trees and spot-5 seasonal time series. Remote Sens Environ 114(3): 552-562.
27. Mutanga O, Adam E, Cho MA (2012) High density biomass estimation for wetland vegetation using worldview-2 imagery and random forest regression algorithm. Int J Appl Earth Obs Geoinf 18: 399-406.
28. Roy DP, Wulder MA, Loveland TR, Allen RG, Anderson MC, et al. (2014) Landsat-8: Science and product vision for terrestrial global change research. Remote Sens Environ 145: 154-172.

How to cite this article: Xuelian M, Haitian Z. Coastal Land Dynamics and Vulnerability Analyses based on the Brightness-Greenness-Wetness Model. Int J Environ Sci Nat Res. 2019; 22(5): 556098. DOI: 10.19080/IJESNR.2019.22.556098

29. Yang J, Weisberg PJ, Bristow NA (2012) Landsat remote sensing approaches for monitoring long-term tree cover dynamics in semi-arid woodlands: Comparison of vegetation indices and spectral mixture analysis. Remote Sens Environ 119: 62-71.

30. Mountrakis G, Im J, Ogole C (2011) Support vector machines in remote sensing: A review. ISPRS J Photogramm Remote Sens 66(3): 247-259.

31. Zhang C, Xie Z (2013) Data fusion and classifier ensemble techniques for vegetation mapping in the coastal everglades. Geocarto Int 29(3): 228-243.

32. Liu QJ, Jing LH, Wang MF, Lin QZ (2013) Hyperspectral remote sensing image classification based on svm optimized by clonal selection. Spectrosc Spect Anal 33: 746-751.

33. Allison MA, Demas CR, Ebersole BA, Kleiss BA, Little CD, et al. (2012) A water and sediment budget for the lower mississippi–atchafalaya river in flood years 2008–2010: Implications for sediment discharge to the oceans and coastal restoration in Louisiana. J Hydrol 432–433: 84-97.

34. Penland S, Beall AD, Britsch LDI, Williams SJ (2002) Geological classification of coastal land loss between 1932 and 1990 in the mississippi river delta plain, southeastern louisiana. Gulf Coast Association of Geological Societies Transactions 52.

35. Theriot JP (2014) American energy, imperiled coast: Oil and gas development in louisiana's wetlands. Louisiana State University Press: Baton Rouge, p. 271.

36. Meng X, Zhang X, Silva R, Li C, Wang L (2017) Impact of high-resolution topographic mapping on beach morphological analyses based on terrestrial lidar and object-oriented beach evolution. ISPRS International Journal of Geo-Information 6: 147.

37. Chang CC, Lin CJ (2011) Libsvm: A library for support vector machines. ACM Transactions on Intelligent Systems and Technology 2: 1-27.

38. Johnson B, Xie Z (2011) Unsupervised image segmentation evaluation and refinement using a multi-scale approach. ISPRS J Photogramm Remote Sens 66(4): 473-483.

39. Fernandez-Manso O, Quintano C, Fernandez-Manso A (2009) Combining spectral mixture analysis and object-based classification for fire severity mapping. Invest Agrar-Sist R 18(3): 296-313.

40. Zhang YL, Lu DS, Yang B, Sun CH, Sun M (2011) Coastal wetland vegetation classification with a landsat thematic mapper image. Int J Remote Sens 32(2): 545-561.

41. Congalton RG, Green K (2008) Assessing the accuracy of remotely sensed data: Principles and practices. CRC press.

42. Jensen JR (2005) Introductory digital image processing: A remote sensing perspective. (3rd edn), Pearson Prentice Hall: Upper Saddle River, NJ.

43. Rouse JW, Haas RH, Schell JA, Deering DW (1974) In Monitoring vegetation systems in the great plains with erts, Proceedings of the Third ERTS Symposium; NASA SP-351, Washington, DC, USA, 1974; NASA Publications: Washington, DC, USA, pp. 309-317.

44. Zha Y, Gao J, Ni S (2003) Use of normalized difference built-up index in automatically mapping urban areas from tm imagery. Int J Remote Sens 24(3): 583-594.

45. Xu H (2006) Modification of normalised difference water index (NDWI) to enhance open water features in remotely sensed imagery. Int J Remote Sens 27(14): 3025-3033.

46. McFeeters SK (1996) The use of the normalized difference water index (NDWI) in the delineation of open water features. Int J Remote Sens 17(7): 1425-1432.

47. Gao B (1996) NDWI—a normalized difference water index for remote sensing of vegetation liquid water from space. Remote Sens Environ 58(3): 257-266.

48. Kauth RJ, Lambeck PF, Richardson W, Thomas GS, Pentland AP (1979) In Feature extraction applied to agricultural crops as seen by landsat, LACIE Symposium, Houston, 1979; ASA. Johnson Space Center Proc. of Tech. Sessions: Houston, pp. 705-721.

49. Crist EP, Kauth RJ (1986) The tasselled cap de-mystified. Photogramm. Eng Remote Sens 52: 81-86.

50. Hsu C, Chang C, Lin C (2010) A practical guide to support vector classification; Taipei City, Taiwan: National Taiwan University.

51. Zhao Q, Bai J, Huang L, Gu B, Lu Q, et al. (2016) A review of methodologies and success indicators for coastal wetland restoration. Ecological Indicators 60: 442-452.

52. (1984) Corps of Engineers, N.O.D., United States. Louisiana coastal area, freshwater diversion to barataria and breton sound basins (feasibility report).

53. Morton RA, Barras JA (2011) Hurricane impacts on coastal wetlands: A half-century record of storm-generated features from southern louisiana. Journal of Coastal Research 27: 27-43.

54. Wikipedia. Hurricanes in louisiana.

55. NOAA (2015) Memorable gulf coast hurricanes of the 20th century.

56. Melton G, Gall M, Mitchell J, Cutter S (2010) Hurricane katrina storm surge delineation: Implications for future storm surge forecasts and warnings. Nat Hazards 54(2): 519-536.

57. Reif MK, Macon CL, Wozencraft JM (2011) Post-katrina land-cover, elevation, and volume change assessment along the south shore of lake pontchartrain, louisiana, USA. Journal of Coastal Research 62: 30-39.

58. Morton RA, Bernier JC, Barras JA (2006) Evidence of regional subsidence and associated interior wetland loss induced by hydrocarbon production, gulf coast region, USA. Environ Geol 50(2): 261-274.

59. Turner RE, Allen RL (1982) Bottom water oxygen concentration in the mississippi river delta bight. Contrib Mar Sci 25: 161-172.

How to cite this article: Xuelian M, Haitian Z. Coastal Land Dynamics and Vulnerability Analyses based on the Brightness-Greenness-Wetness Model. Int J Environ Sci Nat Res. 2019; 22(5): 556098. DOI: 10.19080/IJESNR.2019.22.556098

DOI: 10.19080/IJESNR.2019.21.556098

How to cite this article: Xuelian M, Haitian Z. Coastal Land Dynamics and Vulnerability Analyses based on the Brightness-Greenness-Wetness Model. Int J Environ Sci Nat Res. 2019; 22(5): 556098. DOI: 10.19080/IJESNR.2019.22.556098